HHS Public Access

Author manuscript

Adv Exp Med Biol. Author manuscript; available in PMC 2023 July 03.

Published in final edited form as:

Adv Exp Med Biol. 2021 ; 1269: 23–30. doi:10.1007/978-3-030-48238-1_4.

Updated Evaluation of Cholesterol's Influence on Membrane Oxygen Permeability

Rachel J. Dotson,

Emily McClenahan,

Sally C. Pias*

Department of Chemistry, New Mexico Institute of Mining and Technology (New Mexico Tech), Socorro, NM 87801, U.S.A.

Abstract

There is a surprising gap in knowledge regarding the mechanism of oxygen (O_2) diffusional delivery at the level of tissues and cells. Yet, the effectiveness of tumor radiotherapy, the success of tissue engineering, and healthy metabolism all require ample intracellular oxygen. Tissue-level diffusion takes place in a complex and crowded macromolecular environment. Cholesterol-rich cellular membranes have been thought to reduce oxygen flux. Here, we use atomistic molecular dynamics simulations to update prior estimates of bilayer permeability and related parameters for 1-palmitoyl,2-oleoylphosphatidylcholine (POPC) and POPC/cholesterol bilayers, using a modified O_2 model with improved membrane–water partitioning behavior. This work estimates an oxygen permeability coefficient of 17 ± 2 cm/s for POPC and 12.1 ± 0.4 cm/s for POPC/cholesterol (1:1 molecular ratio) at 37°C. The permeability of POPC is found to be ~1/3 that of a water layer of similar thickness, and the permeability of POPC/cholesterol is estimated to be 20–30% below that of POPC. Void pathway visualization and free energy data support channeling of oxygen toward the center of cholesterol-incorporating membranes, while partition coefficient data suggest reduced membrane solubility of oxygen due to cholesterol. Further study is needed to understand whether diffusion pathway changes due to cholesterol and other molecular compositional factors influence oxygen availability within tissue.

Keywords

Hypoxia; tissue engineering; hydrophobic channeling; simulation; void pathways

1 Introduction

Oxygen (O_2) diffusion across cellular plasma membranes and among intracellular compartments is required for its delivery to tissues. Oxygen delivery in the diffusive regime is especially important where vessels are occluded, damaged, or shunted and where the vessel population is sparse. Clinical conditions affected by tissue-level oxygen diffusion include, for example, diabetic peripheral tissue hypoxia [1], as well as tumor hypoxia

*To whom correspondence should be addressed. sally.pias@nmt.edu. Telephone: +1-575-835-6204.

and associated radiotherapy resistance [2,3]. Cell survival in engineered tissue constructs also depends critically on oxygen diffusion because vessels are generally absent and tissue thicknesses are often in the millimeter range [4].

The rate of diffusive oxygen transport reflects the solubility and diffusion coefficient of O_2 in complex and crowded macromolecular environments. Available diffusion pathways include compositionally complex cellular membranes and protein-crowded cytoplasmic and interstitial fluids. Recent work by our group has focused on clarifying the influence of membrane cholesterol [5] and transmembrane proteins [6] on the kinetics and pathway of oxygen diffusion, using atomistic molecular dynamics simulations. This approach provides atomic resolution insight into the diffusion process, as well as enable calculation of thermodynamic parameters such as free energy.

We previously conducted a simulation study of cholesterol incorporation with the phospholipid 1-palmitoyl,2-oleoylphosphatidylcholine (POPC) [5], which is abundant in eukaryotic plasma membranes. Cholesterol, too, is a normal membrane constituent and typically occurs in the range 20–40% (of the total lipid molecules) in the plasma membranes of most cell types and ~50% in normal red blood cell (RBC) membranes [7,8]. Our study tested the oxygen-permeability effects of 0, 13, 25, 33, 50, and 63% cholesterol in combination with POPC. We additionally tested 100% cholesterol bilayers as a mimic of the noncrystalline cholesterol bilayer domain observed in eye lens fiber cells [9].

The accuracy of POPC and POPC/cholesterol oxygen permeability and partition coefficient estimates calculated from the simulations was evaluated through comparison with experimental data [5]. These comparisons enabled identification of a flaw in the O_2 model, resulting in overestimation of the lipid–water partition coefficient by a factor of 2 or 3. Based on Overton's rule (Eq. 2, below), this overestimation is expected to result in proportional overestimation of bilayer permeability coefficients.

Here, we provide updated estimates of permeability and related parameters for POPC and POPC/cholesterol (50%), using an O_2 model with improved partitioning behavior [10]. In addition, we visualize dynamic void pathways in POPC and POPC/cholesterol (25 or 50%) bilayers. The 50% cholesterol level mimics the lipid composition of red blood cells [8] and eye lens fiber cells [11], while 25% is toward the lower end of the normal cholesterol range of 20–40% for most cell types [7]. Voids, or transiently "empty" volumes, are thought to facilitate solute transport through lipid bilayers. Several studies have quantified voids in phospholipid and phospholipid/cholesterol bilayers [12–15]. Here, time-continuous void pathways within the bilayers are visualized and discussed in relation to oxygen partitioning and permeability.

2 Methods

All-atom molecular dynamics simulations were conducted using graphics processing unit (GPU)-enabled Amber 14 biomolecular simulation software [16,17]. The Lipid14 and ff14SB force fields were used to model lipids and proteins, respectively, along with the TIP3P water model [18–20]. Parameters for modeling O_2 were developed in-house and were

the same as in our earlier work [5], except that some simulations here used an updated oxygen model in which the Lennard-Jones (LJ) well-depth, ε, and interparticle distance of minimum potential energy, r_0, were adjusted to match the values used for the ester carbonyl oxygen atom type (*oC*) in the Lipid14 force field [18]. The updated oxygen model is designated O_2–L14LJ. The earlier model used LJ parameters based on the *o* atom type in the GAFF force field [21] and is designated "O_2–GLJ."

To test the effects of cholesterol on oxygen diffusion, simulations were carried out using lipid bilayers composed of the common membrane phospholipid POPC with varying levels of cholesterol incorporation (0, 25, or 50%). The simulation system compositions are provided in Table 1. Example simulation systems are imaged in Fig. 1, in Results and Discussion, which also illustrates the periodic boundary conditions applied in the simulations.

As previously, the systems were preequilibrated for a minimum of 700 ns [5], and the same preequilibrated bilayers were used as starting structures for simulations with both oxygen models. Each system was simulated without restraints for 300 ns, which was divided into two 150 ns segments for analysis and error estimation. The current simulations used conditions identical to our earlier work [5], except that the method of temperature regulation was varied here, as noted below. Briefly, the simulations were conducted in the isothermal-isobaric (NPT) ensemble, with the temperature maintained at 310 K (37°C) and the pressure at 1.0 bar. The simulation time step was 2 fs, and the SHAKE algorithm [22] was used to constrain all bonds to hydrogen. The Monte Carlo barostat was used for pressure control, with volume change attempts every 100 steps. Temperature regulation was achieved using either the Berendsen weak-coupling thermostat [23] with a coupling constant of 1.0 ps, as previously [5], or Langevin dynamics with a collision frequency of 1.0 ps^{-1}.

The lipid bilayer oxygen permeability, P_M, was assessed by explicitly counting the frequency of O_2 molecule escapes from the bilayer at equilibrium, Φ_{esc}, and normalizing that frequency to the average population of O_2 in the water layer, N_w. Given that the goal was to assess permeability for oxygen *crossing* the bilayer (passing through both leaflets), the number of escapes is also scaled by 1/4 to adjust for counting escapes from both bilayer leaflets (1/2) following entry from either leaflet (1/2). The resulting equation incorporates a factor of 2 correction relative to our earlier work [5]:

$$P_M = \frac{\Phi_{esc}}{4N_w}. \quad (1)$$

Overton's rule predicts the membrane permeability of a solute to be directly proportional to the membrane–water partition coefficient, K_P, and the diffusion coefficient (diffusivity) within the membrane, D_M, but inversely proportional to the membrane thickness, h [24]:

$$P_M = \frac{K_P \cdot D_M}{h}. \quad (2)$$

For a given bilayer, the escape threshold used to obtain Φ_{esc} for Eq. 1 was half the thickness of the lipid bilayer, $\pm h/2$, and was determined as in our earlier study [5]. Bilayer depth-dependent free energy curves, $\Delta G(z)$, were calculated as previously [5]. z is the dimension perpendicular to the plane of the lipid bilayer.

To visualize void pathways across the lipid bilayers, the tunnel analysis software Caver Analyst 1.0 was used [25]. Time series of simulation snapshots from our previous study [5] were analyzed for each bilayer in a series of 10 consecutive frames, spaced 1 ps apart. Time-continuous void pathways were identified using a probe radius of 0.75 Å (~1/3 the radius of an O_2 molecule). This small probe radius generated continuous pathways, which were absent with larger probe size. Though we do not interpret the resulting tunnels to represent actual O_2 migration pathways, very small probe radii have been found to generate void volume fraction profiles [12] similar in shape to oxygen concentration curves [5]. Thus, we expect void pathways associated with the 0.75 Å probe to provide some relevant insight.

3 Results and Discussion

Fig. 1 provides simulation snapshot images for the updated oxygen model (O_2–L14LJ) in hydrated bilayers of POPC alone or with 50% cholesterol (top), along with associated bilayer-depth-dependent free energy curves (middle). Void pathways are also imaged for POPC alone and with 25 or 50% cholesterol (bottom). Table 2 provides permeability coefficients, P_M, and related biophysical parameters, including lipid–water partition coefficients averaged over all bilayer depths, $< K_P >$. Parameters calculated with the original oxygen model, O_2–GLJ, and the updated model, O_2–L14LJ, are compared. Our earlier work [5] used the weak-coupling Berendsen thermostat [23] to control the simulation temperature. Due to concerns of uneven temperature distribution with this thermostat [26], the current work uses Langevin temperature control preferentially. For completeness, Table 2 includes parameters calculated with both thermostats.

First, we note that the simulation snapshot images show concentrating of O_2 molecules toward the bilayer center in the 50% cholesterol system, compared with the POPC system, where the molecules are distributed more evenly throughout the hydrophobic tail region. The free energy curves reflect this shift, showing a narrower and deeper well flanking the bilayer center ($z = 0$ Å). The greater depth of the well in the 50% cholesterol curve indicates greater local lipid–water partitioning of O_2, as the free energy is proportional to the negative logarithm of the local partition coefficient. A similar narrowing is observed in the void-pathway image for 50% cholesterol and, to a lesser extent, for 25% cholesterol, compared with POPC.

The average O_2 lipid–water partition coefficient, $< K_P >$, of 4 ± 1 for the 50% cholesterol bilayer appears lower than that of POPC, at 5 ± 1 (lower part of Table 2, bold type). However, the standard deviation ranges overlap, so the difference may not be significant. Regardless of lipid composition, the $< K_P >$ values obtained with the updated O_2–L14LJ oxygen model are ~1.5 times lower than those in our earlier study with the original O_2–GLJ model (upper part of Table 2, ref. [5]).

Fig. 2 compares the bilayer-depth-dependent partition coefficient, $K_p(z)$, for the original and updated O_2 models with an O_2 partition coefficient curve calculated from experimental nuclear magnetic resonance (NMR) data [27]. It should be noted that the experiment used the phospholipid 1-myristelaidoyl,2-myristoylphosphatidylcholine (MLMPC) at 318 K, while the simulations used POPC at 310 K. Direct correspondence is, thus, not expected. However, the curves should (and do) match in general shape, and the maximum partition coefficient is expected to be similar. The comparison indicates improvement in lipid–water partitioning for O_2–L14LJ, relative to the original O_2 model.

Our previous study showed that addition of 25% cholesterol to POPC reduced the average lipid–water partition coefficient by 39% but did not reduce the bilayer permeability. An explanation for this result is not readily apparent in our data. It is interesting that the void pathways are substantially fewer in the 25% cholesterol bilayer compared with POPC and are more localized to subregions of the bilayer. This effect is amplified in 50% cholesterol, where very few void pathways span the leaflets and where the orientation of the pathways is distinctly perpendicular to the bilayer plane. The latter observation is consistent with the finding of Vattulainen and colleagues that cholesterol incorporation led to fewer voids, which were elongated and primarily oriented normal to the bilayer [13].

The Langevin thermostat is known to dampen diffusive motion, by increasing the apparent viscosity of the medium. For O_2, this effect translates to a downward shift of the bilayer-depth-dependent diffusion coefficient curve [10,28] and an overall reduction of the diffusion coefficient throughout the simulation system. Accordingly, the membrane permeability coefficient values, P_M, are systematically lower for each bilayer simulated with the Langevin thermostat than the same bilayer with the Berendsen barostat (Table 2). Assessment of the updated O_2–L14LJ model indicates that the lipid–water partition coefficient remains overestimated (Fig. 2 and ref. [10]). As such, with respect to the permeability coefficient, it appears there may be cancellation of errors due to underestimated diffusion coefficient and overestimated partition coefficient.

With the Langevin thermostat and the updated oxygen model O_2–L14LJ, the permeability is estimated to be 17.0 ± 1.5 cm/s for POPC and 12.1 ± 0.4 cm/s for 50% cholesterol (lower part of Table 2). These values are consistent in trend with those reported in our earlier study (Berendsen thermostat, upper half of Table 2) but are ~1.5 times lower in magnitude. The current permeability values are also consistent in trend with values in another study in this volume for POPC alone and with 50% cholesterol at 37°C, calculated independently using the updated oxygen model O_2–L14LJ [29]. However, that study used a distinct bilayer equilibration protocol and yielded a permeability value of 7.9 ± 0.2 cm/s for 50% cholesterol, 46% lower than the associated POPC value of 14.6 ± 0.4 cm/s, which falls at the lower end of the present error range.

The ratio P_M/P_w provides a useful, thickness-independent means of comparing the permeabilities of various bilayers. P_w is the permeability of a water layer of the same thickness as a given bilayer and here is calculated using the simulation bilayer thickness, h, combined with an experimental value for the oxygen diffusion coefficient in pure water. P_M/P_w additionally enables evaluation of the permeability of a given bilayer relative to the

permeability of unstirred water. With the updated oxygen model, P_M/P_w indicates POPC to have ~1/3 the permeability of a water layer of the same thickness, compared with a somewhat lower value of 0.28 for 50% cholesterol.

4 Conclusions

The current study provides updated estimates of the transbilayer oxygen permeability of POPC and 50% cholesterol bilayers. The permeability coefficients use a corrected equation and an updated simulation O_2 model, along with the more thermodynamically rigorous Langevin thermostat. The POPC bilayer, at 17 cm/s, is estimated to be about 1/3 as permeable as a water layer of the same thickness, while POPC with 50% cholesterol is estimated to be 20–30% less permeable than POPC (or possibly as much as 46% less, based on related calculations in ref. [29]). These permeabilities are expected to have a direct influence on transbilayer oxygen flux.

In a tissue-level diffusion scheme dominated by water-based pathways (interstitial fluid and cytoplasm), the membrane permeabilities calculated here would not be rate-limiting [5]. Membrane proteins have not been accounted for here but have been included in our recent work [6]. Their influence is substantial, yet we have no indication, thus far, that even protein-rich membranes would be rate-limiting for aqueous-dominated diffusion. It is important to consider, however, that experimental and theoretical evidence points toward lipid-mediated diffusion pathways [30]. In such a scheme, the radial diffusion coefficient [31] and interleaflet solubility of oxygen would likely play a role in determining the magnitude of oxygen flux to subcellular compartments within tissue. As such, further study of lipid-mediated oxygen diffusion and assessment of the permeability of protein crowded aqueous fluids and membranes is needed.

Acknowledgments

The authors thank Richard Pastor for helpful comments on the manuscript. The research was enabled by an IDeA award from the National Institute of General Medical Sciences of the National Institutes of Health (P20GM103451) and by a gift from the Glendorn Foundation. VMD [32] software was used to generate the simulation system images.

References

1. Cicco G; Giorgino F; Cicco S Wound healing in diabetes: Hemorheological and microcirculatory aspects. Adv. Exp. Med. Biol. 2011, 701, 263–269. [PubMed: 21445796]
2. Multhoff G; Radons J; Vaupel P Critical role of aberrant angiogenesis in the development of tumor hypoxia and associated radioresistance. Cancers (Basel). 2014, 6 (2), 813–828. [PubMed: 24717239]
3. Hou H; Dong R; Lariviere JP; et al. Synergistic combination of hyperoxygenation and radiotherapy by repeated assessments of tumor pO2 with EPR oximetry. J. Radiat. Res. 2011, 52 (5), 568–574. [PubMed: 21799293]
4. Rouwkema J; Koopman BF, Blitterswijk JM, Van CA; et al. Supply of nutrients to cells in engineered tissues. Biotechnol. Genet. Eng. Rev. 2009, 26 (1), 163–178.
5. Dotson RJ; Smith CR; Bueche K; et al. Influence of cholesterol on the oxygen permeability of membranes: Insight from atomistic simulations. Biophys. J. 2017, 112 (11), 2336–2347. [PubMed: 28591606]

6. Dotson RJ; Pias SC Reduced oxygen permeability upon protein incorporation within phospholipid bilayers. Adv. Exp. Med. Biol. 2018, 1072, 405–411. [PubMed: 30178379]
7. Mouritsen OG; Zuckermann MJ What's so special about cholesterol? Lipids 2004, 39 (11), 1101–1113. [PubMed: 15726825]
8. Jandl JH Blood: Textbook of Hematology, 2nd ed.; Little, Brown and Company: Boston, MA, 1996.
9. Raguz M; Mainali L; Widomska J; Subczynski WK The immiscible cholesterol bilayer domain exists as an integral part of phospholipid bilayer membranes. Biochim. Biophys. Acta Biomembr. 2011, 1808 (4), 1072–1080.
10. Dotson RJ; Shea R; Byrd E; Pias SC Optimization of an additive molecular oxygen model for membrane simulation studies. In preparation.
11. Widomska J; Raguz M; Subczynski WK Oxygen permeability of the lipid bilayer membrane made of calf lens lipids. Biochim. Biophys. Acta 2007, 1768 (10), 2635–2645. [PubMed: 17662231]
12. Marrink SJ; Sok RM; Berendsen HJC Free volume properties of a simulated lipid membrane. J. Chem. Phys. 1996, 104 (22), 9090–9099.
13. Falck E; Patra M; Karttunen M; et al. Impact of cholesterol on voids in phospholipid membranes. J. Chem. Phys. 2004, 121, 12676–12689. [PubMed: 15606294]
14. Mahinthichaichan P; Gennis RB; Tajkhorshid E All the O2 Consumed by Thermus thermophilus Cytochrome ba3 Is Delivered to the Active Site through a Long, Open Hydrophobic Tunnel with Entrances within the Lipid Bilayer. Biochemistry 2016, 55 (8), 1265–1278. [PubMed: 26845082]
15. Chipot C; Comer J Subdiffusion in Membrane Permeation of Small Molecules. Sci. Rep. 2016, 6, 1–14. [PubMed: 28442746]
16. Case DA; Berryman JT; Betz RM; et al. AMBER 2015; University of California, San Francisco, 2015.
17. Salomon-Ferrer R; Götz AW; Poole D; et al. Routine microsecond molecular dynamics simulations with AMBER on GPUs. 2. Explicit solvent particle mesh Ewald. J. Chem. Theory Comput. 2013, 9 (9), 3878–3888. [PubMed: 26592383]
18. Dickson CJ; Madej BD; Skjevik ÅA; et al. Lipid14: The Amber lipid force field. J. Chem. Theory Comput. 2014, 10 (2), 865–879. [PubMed: 24803855]
19. Maier JA; Martinez C; Kasavajhala K; et al. ff14SB: Improving the accuracy of protein side chain and backbone parameters from ff99SB. J. Chem. Theory Comput. 2015, 11 (8), 3696–3713. [PubMed: 26574453]
20. Jorgensen WL; Chandrasekhar J; Madura JD; et al. Comparison of simple potential functions for simulating liquid water. J. Chem. Phys. 1983, 79 (2), 926.
21. Wang J; Wolf RM; Caldwell JW; et al. Development and testing of a general Amber force field. J. Comput. Chem. 2004, 25 (9), 1157–1174. [PubMed: 15116359]
22. Ryckaert J-P; Ciccotti G; Berendsen HJC Numerical integration of the Cartesian equations of motion of a system with constraints: Molecular dynamics of n-alkanes. J. Comput. Phys. 1977, 23 (3), 327–341.
23. Berendsen HJC; Postma JPM; van Gunsteren WF; et al. Molecular dynamics with coupling to an external bath. J. Chem. Phys. 1984, 81 (8), 3684.
24. Missner A; Pohl P 110 Years of the Meyer-Overton rule: Predicting membrane permeability of gases and other small compounds. Chem Phys Chem 2009, 10 (9–10), 1405–1414. [PubMed: 19514034]
25. Kozlikova B; Sebestova E; Sustr V; et al. CAVER Analyst 1.0: Graphic tool for interactive visualization and analysis of tunnels and channels in protein structures. Bioinformatics 2014, 30 (18), 2684–2685. [PubMed: 24876375]
26. Feller SE; Zhang Y; Pastor RW; Brooks BR Constant pressure molecular dynamics simulation: The Langevin piston method. J. Chem. Phys. 1995, 103 (11), 4613.
27. Al-Abdul-Wahid MS; Yu CH; Batruch I; et al. A combined NMR and molecular dynamics study of the transmembrane solubility and diffusion rate profile of dioxygen in lipid bilayers. Biochemistry 2006, 45 (35), 10719–10728. [PubMed: 16939224]
28. Gaalswyk K; Awoonor-Williams E; Rowley CN Generalized Langevin Methods for Calculating Transmembrane Diffusivity. J. Chem. Theory Comput. 2016, 12 (11), 5609–5619.

29. Wang Q; Dotson RJ; Angles G; Pias SC Simulation study of breast cancer lipid changes affecting membrane oxygen permeability: Effects of chain length and cholesterol. Adv. Exp. Med. Biol. 2020.

30. Pias SC Pathways of oxygen diffusion in cells and tissues: Hydrophobic channeling via networked lipids. Adv. Exp. Med. Biol.

31. Ghysels A; Venable RM; Pastor RW; Hummer G Position-dependent diffusion tensors in anisotropic media from simulation: Oxygen transport in and through membranes. J. Chem. Theory Comput. 2017, 13, 2962–2976. [PubMed: 28482659]

32. Humphrey W; Dalke A; Schulten K VMD - Visual Molecular Dynamics. J. Mol. Graph. 1996, 14, 33–38. [PubMed: 8744570]

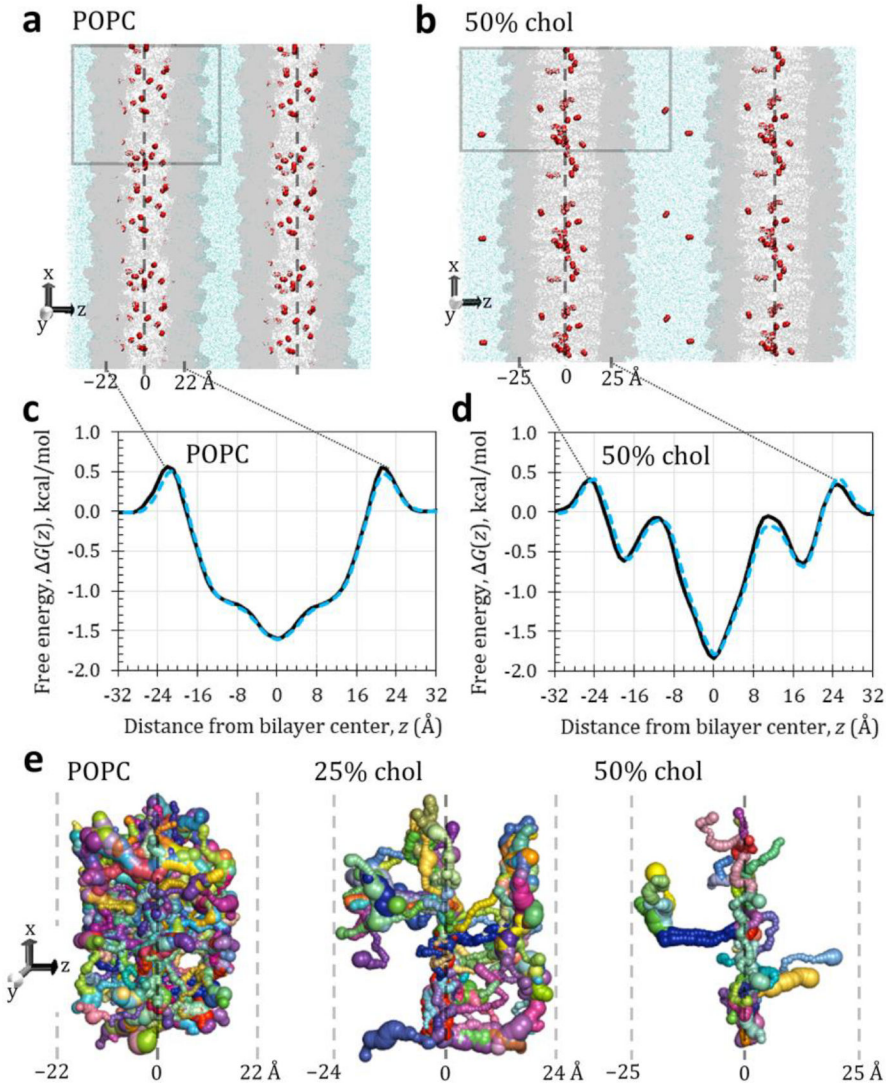

Fig. 1.

(a, b) Representative simulation snapshots for POPC and 50% cholesterol, showing the primary simulation box (gray outline) with composition specified in Table 1 and adjacent images to illustrate the periodic boundary conditions. The simulation "sees" an infinitely wide bilayer in both *x* and *y* dimensions and an infinite number of membrane and water layers in the *z* dimension. O_2 molecules visualized as red spheres, water as light blue dots. POPC and cholesterol shown in gray (darker areas are POPC headgroups). Labels indicate approximate positions of bilayer center and headgroup-associated free energy barriers. Dashed line indicates bilayer center. **(c, d)** Relative bilayer-depth-dependent free energy curves for O_2 in POPC and 50% cholesterol, using the Langevin thermostat (black lines) or the Berendsen thermostat (dotted blue lines). **(e)** Void pathways within each bilayer, oriented as in panel b but displayed at larger scale. Shown are continuous pathways generated from 10 consecutive trajectory snapshots spaced 1 ps apart (covering 10 ps of simulation time), using a 0.75-Å probe to identify empty volumes transiently devoid of atoms. Voids large enough to contain the probe are pictured as spheres, which are connected into pathways

through occurrence of neighboring voids in consecutive snapshots. Sphere size represents void volume. Locally continuous pathway segments are distinguished by color. Labels and dashed lines indicate approximate bilayer-depth positions in ångströms.

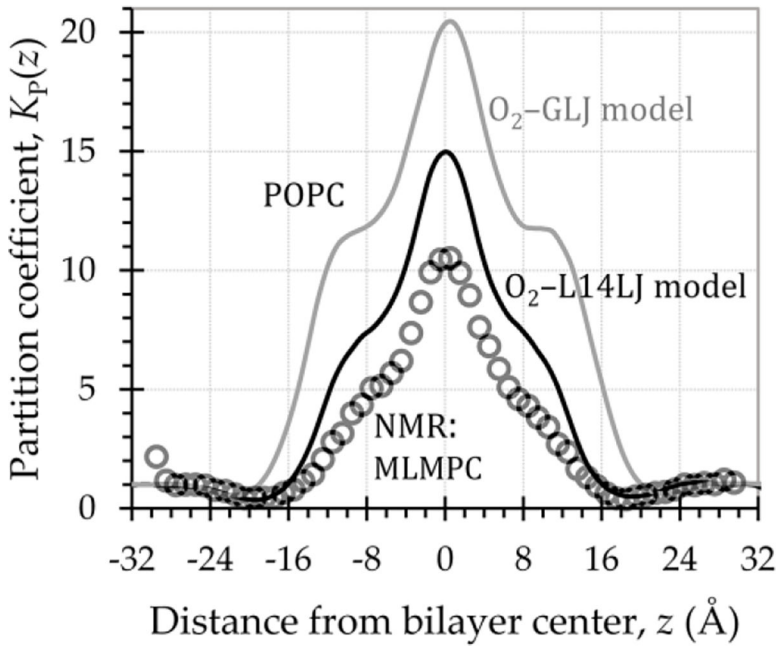

Fig. 2.

Depth-dependent O_2 lipid–water partition coefficient curves, $K_P(z)$, showing improved partitioning for the updated O_2–L14LJ model (black line), relative to the original O_2–GLJ model (gray line). Circles represent $K_P(z)$ calculated from experimental NMR data [27], for O_2 in MLMPC at 318 K. Simulations used POPC at 310 K, with Langevin temperature control (collision frequency 1.0 ps^{-1}) and the Monte Carlo barostat.

Table 1

Simulation system compositions (number of molecules) and bilayer areas, A_{bil}

System name	POPC	Cholesterol	Water	O_2	A_{bil} (Å^2) Langevin	A_{bil} (Å^2) Berendsen
POPC	128	0	4,445	35	4,095	4,142
25% chol	96	32	4,447	33	Not applicable.	3,241
50% chol	64	64	4,449	31	2,698	2,722

Mean A_{bil} from simulations with Langevin or Berendsen thermostat, standard deviation ≤ 12 Å^2.

Table 2

Comparison of permeability and related biophysical parameters calculated with the original and updated O_2 models, at 37°C with two different simulation thermostats

System	Thermostat	P_M (cm/s)	h (Å)	P_w (cm/s)	P_M/P_w	$< K_P >$
Original oxygen model, O2-GLJ						
POPC	Berendsen [a]	26 ± 2	56	46	0.57	8.0 ± 0.5
	Langevin	21 ± 3	54	48	0.44	8.6 ± 0.1
25% chol	Berendsen [a]	24 ± 2	60	43	0.56	6.2 ± 0.1
50% chol	Berendsen [a]	21 ± 1	60	43	0.49	5.0 ± 0.0
Updated oxygen model, O_2-L14LJ						
POPC	Berendsen	18.0 ± 0.7	56	46	0.39	4.9 ± 0.3
	Langevin	**17.0 ± 1.5**	**54**	**48**	**0.35**	**5 ± 1**
50% chol	Berendsen	17.1 ± 0.8	60	43	0.40	3.4 ± 0.2
	Langevin	**12.1 ± 0.4**	**60**	**43**	**0.28**	**4 ± 1**

Values shown as mean ± standard deviation, where applicable. P_M: membrane O_2 permeability coefficient. h: bilayer thickness. P_w: permeability of an unstirred water layer of the same thickness as the respective bilayer, calculated as $P_w = D_w/h$, where $D_w = 2.60 \times 10^{-5}$ cm^2/s is the experimental diffusion coefficient for O_2 in water at 37°C (see ref. [5]). $< K_P >$: lipid-water partition coefficient averaged over all bilayer depths.

[a] Data in these rows from ref. [5]. P_M values corrected by a factor of 2, as in Eq. 1.